IEEE Access
Multidisciplinary | Rapid Review | Open Access Journal

Received September 13, 2019, accepted October 5, 2019, date of publication October 11, 2019, date of current version October 23, 2019.

Digital Object Identifier 10.1109/ACCESS.2019.2946972

Enhanced Robust Deadbeat Predictive Current Control for PMSM Drives

XIN YUAN, SHUO ZHANG, (Member, IEEE), AND CHENGNING ZHANG
National Engineering Laboratory for Electric Vehicles, School of Mechanical Engineering, Beijing Institute of Technology, Beijing 100081, China
Corresponding author: Shuo Zhang (shuozhangxd@gmail.com)

ABSTRACT In permanent-magnet synchronous machine (PMSM) applications, traditional deadbeat predictive current control (DPCC) utilizes the PMSM model to evaluate the expected voltage vector and applies it to the inverter through space vector pulse width modulation (SVPWM). Once the expected voltage vector is inaccurate, the torque ripple and speed fluctuation are amplified. There are two main factors that cause the inaccurate voltage vector, namely model parameter mismatch, and current measurement error. To enhance the robustness of DPCC, first, this paper proposes an accurate PMSM voltage model with nonperiodic and periodic disturbance models. Second, this paper proposes a novel current and disturbance observer (NCDO) which is able to predict future stator currents and disturbances caused by model parameter mismatch and current measurement error simultaneously. Finally, the scheme of the proposed DPCC with NCDO is presented to enhance the robustness. This paper presents a comparative study of two types of algorithms, namely traditional DPCC and the proposed DPCC with NCDO. The theoretical verification, simulation results, and experimental results are demonstrated to verify the effectiveness of the proposed DPCC with NCDO.

INDEX TERMS Permanent-magnet synchronous machine (PMSM), deadbeat predictive current control (DPCC), iterative learning control (ILC), sliding-mode control (SMC).

I. INTRODUCTION

Recently, permanent-magnet synchronous machines (PMSMs) have been widely used in the modern applications because they have a range of benefits such as high efficiency, high torque density, and excellent control precision. To achieve high steady-state and dynamic performance, some control strategies have been applied in the drive system of PMSMs, such as classical proportional–integral (PI) control [1], hysteresis control, and predictive control.

A. LITERATURE REVIEW

Hysteresis control [2] has good robustness, fast current responses, and simple computation, but there are large current ripples in the control system. Compared with hysteresis control, PI control has some benefits such as small current ripples and fixed switching frequency, which is popular in practical applications. However, the PI parameters need to be tuned, which is time-consuming. Recently, predictive control is applied in PMSM drives within ten years. Predictive control has some advantages, such as excellent performance in the transient state [3]. It can be categorized into two types of predictive control normally, namely finite control set model predictive control (FCS-MPC) [4] and deadbeat predictive control (DPCC). FCS-MPC applies finite voltage vectors based on characteristic of inverters to predict next instant motor stator currents by minimizing cost functions. However, limited voltage vectors can lead to large current ripples compared with DPCC. DPCC is based on a discrete mathematical model to predict a voltage vector and apply it to the inverter through space vector pulse width modulation (SVPWM) [5].

There has been extensive research in the area of predictive control. Disturbance suppression is quite significant in predictive control since DPCC bases the motor model parameters to control the motor. To deal with the disturbances in the field of PMSM drives, many methods have been proposed. Reference [6] proposed model-free control strategies that can suppress parameter mismatch disturbances. This method can predict the next instant voltage vectors based on current sampling information, but there is a stagnant current update in the algorithm. In order to deal with this problem, [7] proposed an improved

The associate editor coordinating the review of this manuscript and approving it for publication was Ning Sun.

model-free control. The specific procedure is to conduct two current measurements within each sampling period, the second of which is delayed for a fixed time after the switching state begins, but this method may lead to current spikes. Reference [8] proposed an improved model-free control with single-current sampling technology, which can reduce current ripples. In addition to model-free control strategies, [9] proposed a novel speed-control method composed of an adaptive feedforward control term, which compensates for the nonlinear and uncertain factors. Reference [10] proposed a novel estimator based on the model reference adaptive system for online estimation and tracking of stator resistance, which can overcome the motor resistance mismatch disturbance. However, this method cannot deal with inductance mismatch disturbance. Reference [11] developed a reduced-order observer to suppress the inductance mismatch disturbances, but the disturbance estimation is imprecise and time-consuming. References [12], [13] proposed predictive control with current errors to modify the motor model continually, which can suppress the model parameter disturbances. However, it is only applied in FCS-MPC applications instead of with DPCC. Reference [14] proposed a lunenberger disturbance observer based on Xilinx Zynq SoC XC7Z020-CLG484-1 and FPGA implementations to estimate the lumped disturbances in the speed and current loops. In addition, [15] proposed a novel generalized proportional integral observer to estimate disturbances caused by machine model parameters.

It is generally known that sliding-mode control (SMC) is a type of nonlinear control to deal with nonperiodic disturbances. Reference [16] proposed a nonlinear speed-control algorithm with an SMC disturbance observer, but it is mainly applied in the PI speed controller. Reference [17] proposed an improved DPCC combined with a second-order SMC disturbance observer for a PMSM drive to reduce current harmonics, but the algorithm is quite complex and time-consuming. To reduce computation, [18] proposed a first-order SMC disturbance observer to estimate the parameter mismatch disturbances. However, it is hard to suppress disturbances due to currents measurement errors because the switching gain in the SMC becomes large when the value of disturbances increases, which can cause sliding-mode chattering.

In the traditional DPCC, the current sampling information is significant since the disturbances can lead to speed pulsation [19]. Thus, the current sampling error needs to be reduced to increase the DPCC performance. The current sampling errors mainly include current-measurement offset and scaling errors, which belongs to periodic disturbances. To deal with the disturbances, [20] proposed a speed-control method for PMSMs with iterative learning control (ILC) [21]. ILC is a method of tracking control for systems that work in a repetitive mode. By incorporating feedback, ILC has better robustness compared with other feedforward control methods [22]–[24]. Reference [25] proposed a novel speed controller with an ILC module and adaptive SMC observer, but [25] focused on a speed controller in which the controlled output is the q-axis current reference and the current controller is still a traditional PI regulator, which is not suitable for DPCC.

B. MOTIVATION AND INNOVATION

Because the traditional DPCC mainly based on model parameter and current measurement information, the challenges of the traditional DPCC is to suppress the disturbances caused by model parameters mismatch and current measurement errors simultaneously. The method of [25] can suppress both but it is not suitable for DPCC. To overcome the aforementioned drawbacks in the traditional DPCC, the new DPCC scheme is proposed in this paper. In the proposed DPCC scheme, it can suppress the parameter model disturbance and current sampling disturbance simultaneously.

There are four contributions in this paper. (1) An accurate PMSM model considering the influence of parameter mismatches and measurement errors is analyzed and a modified DPCC that contains an accurate PMSM voltage model and nonperiodic and periodic disturbance models is proposed. (2) Unlike previous studies, which added the ILC module into the speed controller, this paper takes the predicted periodic disturbances $f'_{i+1}(\theta_e)$ as the controlled output in the modified DPCC, and the ILC law is different from that in the previous study. (3) This paper proposes a novel current and disturbance observer (NCDO) in the modified DPCC. The disturbances that the NCDO predicts are regarded as the feedforward voltage compensation and are directly added into a modified PMSM voltage model, which is different from the speed controller in [25]. The proposed disturbance observer can predict the total disturbances and the stator currents at the next time, which can operate well with a modified DPCC. (4) The simulation and experimental results are demonstrated to verify the performance of the proposed DPCC with NCDO under parameters mismatch and current-measurement error conditions.

C. PAPER ORGANIZATION

This paper is organized as follows. Section II illustrates the principle of DPCC and the accurate PMSM model considering parameters mismatches and current measurement errors. Then, the proposed DPCC with NCDO is shown in Section III. Section IV and V present the simulation and experimental results for the traditional DPCC and the proposed DPCC with NCDO. Finally, the conclusions are presented in Section VI.

II. DEADBEAT PREDICTIVE CURRENT CONTROL

In the traditional DPCC, the expected voltage vector is obtained through motor mathematical model. In this section, first, the mathematical model of PMSM is introduced and then the principle of the traditional DPCC is presented. Finally, an accurate PMSM model under the influence of parameters mismatches and current measurement errors is analyzed and established.

A. MATHEMATICAL MODEL OF PMSM

This paper chooses the surface-mounted PMSM as the research target and ignores some trivial parameters of PMSM. Therefore, the mathematical model of the PMSM equations can be presented as

$$U_{\mathrm{s}} = R_{\mathrm{s}} i_s + \frac{d\psi_s}{dt} \tag{1}$$

$$\psi_s = L_{\mathrm{s}} i_s + \psi_{\mathrm{m}} e^{j\theta_r} \tag{2}$$

$$T_{\mathrm{e}} = 1.5 p \psi_{\mathrm{m}} i_q \tag{3}$$

where R_{s}, L_{s}, and Ψ_{m} denote the PMSM stator resistance, stator inductance, and rotor flux linkage, respectively; i_{s} and U_{s} stand for the stator current vectors and stator voltage vectors, respectively; p *and* θ_{r} are the number of pole pairs and electrical rotor angle, respectively; and Ψ_{s} denotes the stator flux vector. The mechanical equation of PMSM can be expressed as

$$T_{\mathrm{e}} - T_l = \eta \frac{d\omega_m}{dt} \tag{4}$$

where T_{e} denotes the electromagnetic torque, η stands for machine inertia, ω_{m} stands for the PMSM mechanical rotor speed, and T_l stands for load torque.

B. PRINCIPLE OF DPCC

The principle of DPCC is to utilize motor voltage equation to obtain the expected voltage vector. According to Eq. (1) and Eq. (2), the PMSM voltage equation on stationary frame can be presented as

$$U_s = R_s i_s + L_s \frac{di_s}{dt} + j\psi_m \omega_m p e^{j\theta_r} \tag{5}$$

In the digital system, the selected voltage vector using measurements at the kth instant will continue being applied after (k+1)th instant. In this case, delay compensation needs to be considered, and the specific procedure can be expressed as follows.

First, based on [26], the delay compensation should be applied in DPCC. In this case, to reduce the calculation, this paper adopts the first-order Euler discretization to acquire the next time stator current i_{s}(k+1), which can be expressed as

$$i_s(\mathrm{k+1}) = i_s(\mathrm{k}) + \frac{\mathrm{T}_s}{L_s}\left(U_{\mathrm{s}}(\mathrm{k})^* - R_s i_s(\mathrm{k}) - j\psi_m \omega_m p e^{j\theta_r}\right) \tag{6}$$

where $U_{\mathrm{s}}(\mathrm{k})^*$ denotes the known voltage vectors at the kth instant. After obtaining the stator currents i_{s}(k+1) at the (k+1)th instant, the voltage equation at the (k+1)th instant can be expressed as

$$U_{\mathrm{s}}(\mathrm{k+1}) = \frac{L_s}{\mathrm{T}_s} i_s^{\mathrm{ref}}(\mathrm{k+2}) - \frac{L_s}{\mathrm{T}_s} i_s(\mathrm{k+1}) + R_s i_s(\mathrm{k+1}) + j\psi_m \omega_m p e^{j\theta_r} \tag{7}$$

Because the sampling period is quite short, this paper neglects the variation in θ_{r} between the (k+1)th instant and the kth instant. Therefore, the amplitude of the reference stator currents $i_{\mathrm{s}}^{\mathrm{ref}}$(k+2) is equal to the amplitude of reference stator currents $i_{\mathrm{s}}^{\mathrm{ref}}$(k+1), which can be presented as

$$i_s^{\mathrm{ref}}(\mathrm{k+2}) = i_s^{\mathrm{ref}}(\mathrm{k+1}) \tag{8}$$

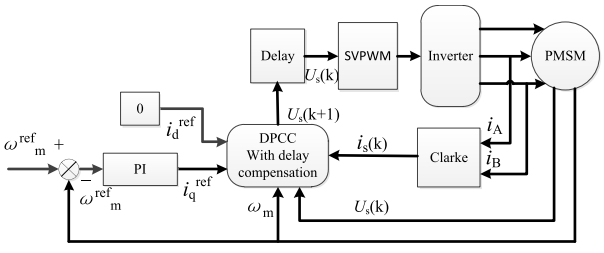

FIGURE 1. The traditional DPCC scheme of PMSM drives.

Substituting Eq. (6) and Eq. (8) into Eq. (7), the desired voltage vector is obtained and be applied in inverter through SVPWM modulation. The traditional DPCC scheme of PMSM drive is presented in Fig. 1, where delay block stands for a one-step delay in practical system.

C. ESTABLISHMENT OF ACCURATE MATHEMATICAL MODEL

According to Eq. (5), there are some PMSM parameters including the resistance, inductance, and flux linkage parameters. These values might not be determined precisely, and sometimes the values might change during operation. The parameter mismatch disturbances will have adverse impacts on the performance of motor operation.

In addition to parameter mismatch disturbances, there are some periodic disturbances. For example, stator currents are measured through the Hall sensor or high-precision resistance, which can lead to periodic measurement errors. The currents measurement errors include current dc offsets and scaling errors. Reference [25] presented that dc offsets can cause the measured current error in the dq coordinates to oscillate at the electrical angle frequency and the scaling errors can cause the measured current error in the dq coordinates to oscillate at twice the electrical angle frequency. Previous analysis shows that measured currents consist of a fundamental component together with the 1st- and 2nd-harmonic components, which are periodic current ripples. The currents can be expressed as Eq. (9) and Eq. (10).

$$i_{dm} = \left\| i_d^0 \right\| + \left\| i_d^1 \right\| \sin(\theta_e) + \left\| i_d^2 \right\| \sin(2\theta_e) \tag{9}$$

$$i_{qm} = \left\| i_q^0 \right\| + \left\| i_q^1 \right\| \sin(\theta_e) + \left\| i_q^2 \right\| \sin(2\theta_e) \tag{10}$$

where $||i_d^0||$ and $||i_q^0||$ are the dc components; $||i_d^1||$, $||i_d^2||$, $||i_q^1||$, and $||i_q^2||$ denote the 1st- and 2nd-harmonic current amplitudes of the periodic disturbances in the dq coordinates; i_{dm} and i_{qm} are crude measured currents, which contain a dc component and periodic components; and θ_{e} denotes the electrical angle of the harmonic current. In particular, when the crude measured current i_{qm} is taken as the feedback current, it generates the 1st- and 2nd-harmonic pulsating torque T_0. T_1 is the dc-offset torque caused by $||i_q^0||$, which can be expressed as Eq. (11). The 1st- and 2nd-harmonic current torque T_0

can lead to motor speed fluctuation according to Eq. (4). Therefore, to increase the robustness of DPCC, the suppression of stator current measurement error is crucial.

$$T_e = T_1 + T_0 \tag{11}$$

Considering parameter mismatch and current measurement error disturbances, the accurate PMSM mathematical model is established in this paper. The accurate PMSM voltage equations in the dq coordinates can be expressed as

$$\begin{cases} U_d = L_s' \dfrac{di_{dm}}{dt} + R_s' i_{dm} - \omega_m p L_s' i_{qm} + r_d - f_d \\ r_d = \Delta L_s \dfrac{di_{dm}}{dt} + \Delta R_s i_{dm} - \omega_m p \Delta L_s i_{qm} \\ f_d = L_s \dfrac{d\Delta i_{dm}}{dt} + R_s \Delta i_{dm} - \omega_m p L_s \Delta i_{qm} \end{cases} \tag{12}$$

$$\begin{cases} U_q = L_s' \dfrac{di_{qm}}{dt} + R_s' i_{qm} + \omega_m p L_s' i_{dm} + \omega_m p \psi_m' + r_q - f_q \\ r_q = \Delta L_s \dfrac{di_{qm}}{dt} + \Delta R_s i_{qm} + \omega_m p \Delta L_s i_{dm} + \omega_m p \Delta \psi_m \\ f_q = L_s \dfrac{d\Delta i_{qm}}{dt} + R_s \Delta i_{qm} + \omega_m p L_s \Delta i_{dm} \end{cases} \tag{13}$$

where L_s', R_s', and Ψ_m' are the crude motor parameters that are measured initially; ΔL_s, ΔR_s, $\Delta \Psi_m$ are the variation of the motor parameters; and L_s, R_s, and Ψ_m are the actual motor parameters. In this case, $L_s = L_s' + \Delta L_s$, $R_s = R_s' + \Delta R_s$, and $\Psi_m = \Psi_m' + \Delta \Psi_m$; and r_d and r_q denote the nonperiodic disturbances of parameter variations. Furthermore, Δi_{dm} and Δi_{qm} are current ripple variations, and i_d and i_q are real stator currents. In this case, $i_d = i_{dm} - \Delta i_{dm}$ and $i_q = i_{qm} - \Delta i_{qm}$, and f_d and f_q denote the periodic disturbances of current measurement error.

III. PROPOSED DPCC WITH NCDO

After obtaining the accurate PMSM model, it can be seen that the stator current, periodic disturbances f_d and f_q, and nonperiodic disturbances r_d and r_q at the (k+1)th instant need to be predicted in the modified DPCC. Therefore, this paper proposes NCDO to satisfy the needs of the modified DPCC. The pioneering study shows that ILC can suppress the periodic disturbances and SMC can deal with parameter disturbances. The difficulty encountered in this research is that the periodic and nonperiodic disturbances are difficult to be suppressed at the same time.

In this case, NCDO can be designed to have the features of both ILC and SMC. First, the principle of an improved ILC module needs to be presented.

The principle of ILC is to learn and amend the controlled output according to the last and the present controlled input during every iteration cycle. After several iteration cycles, the learned and amended controlled outputs are predicted to end. According to the aforementioned analysis, currents measurement error can lead to pulsating torque according to Eq. (3), which can in turn lead to pulsating speed according to Eq. (4). Unlike the other study on ILC, which took the q-axis reference current as the controlled output, this paper takes the predicted disturbances voltage $f_{i+1}'(\theta_e)$ as the controlled output and takes the mechanical rotor speed error as the controlled input. Furthermore, because the differential of mechanical rotor speed is linked to the torque ripple, to confirm the convergence of ILC, the proportional–differential (PD) type ILC law can be taken as the ILC law. The diagram of the proposed ILC module is shown in Fig. 2 and the proposed ILC formula can be expressed as Eq. (14).

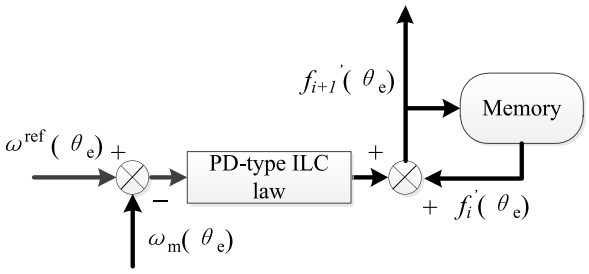

FIGURE 2. Schematic diagram of PD-type ILC module.

$$f_{i+1}'(\theta_e) = f_i'(\theta_e) + k_{f1} \frac{d\left(\omega_m(\theta_e)_i - \omega^{ref}(\theta_e)_i\right)}{dt} + k_{f2} \frac{d\left(\omega_m(\theta_e)_{i+1} - \omega^{ref}(\theta_e)_{i+1}\right)}{dt} \tag{14}$$

where θ_e denotes the electrical angle of periodic disturbances, i represents the ith iteration cycle, and there are several system sampling periods per iteration cycle. Because the disturbances of current-measurement error have periodic characteristics, $f_{i+1}'(\theta_e) = f_{i+1}'(2\pi + \theta_e)$; k_{f1} and k_{f2} denote ILC parameters and the selection principle of parameters is introduced in Section III-B; $f_{i+1}'(\theta_e)$ denotes the controlled output in the $(i+1)$th iteration cycle. The initial controlled output value of $f_i'(\theta_e)$ is zero and it is assumed that the desired motor rotor speed is differentiable with the change in time t. Because the motor speed pulsations are periodic with respect to the motor electrical angle, the learning update mechanism learns and amends the controlled output $f_{i+1}'(\theta_e)$ according to the electrical angle θ_e instead of time t. Through memory-based learning, $f_{i+1}'(\theta_e)$ is stored in memory during the entire iteration cycle and is used for the next iteration cycle.

It has been noted that the ILC-controlled output $f_{i+1}'(\theta_e)$ can be obtained when the system operates at steady state for several iteration cycles, and if the system operates in the transient state, the ILC-controlled output $f_{i+1}'(\theta_e)$ cannot be obtained and the value $f_{i+1}'(\theta_e)$ remains zero. The ILC controlled output $f_{i+1}'(\theta_e)$ can be regarded as the predicted feedforward voltage compensation f_d and f_q, which can be applied directly in the inverter through SVPWM. Actually, the proposed ILC would study and amend the disturbances caused by q-axis current ripple. For example, the proposed ILC can predict the actual resistance feedforward voltage compensation caused by q-axis current ripple. Whereas in

traditional ILC, as described by [25], the controlled output is the q-axis reference current, it can only predict the crude resistance voltage compensation because the actual resistance parameters cannot be obtained. Therefore, the traditional ILC is only suitable for PI current controllers under parameter mismatch. Overall, the proposed method can study and amend the voltage compensation, and the voltage compensation can be regarded as the feedforward compensation. The compensation can generate pulsating torque, as indicated by Eq. (11), that can counteract the pulsating torque T_0 caused by the 1st- and 2nd-harmonic currents $||i_d^1||$, $||i_d^2||$, $||i_q^1||$, and $||i_q^2||$, as in Eq. (9) and Eq. (10). Furthermore, the proving process is introduced in Section III-B.

After introducing the ILC module, the SMC module is proposed to suppress nonperiodic disturbances in NCDO and acquire the predicted stator currents i_d(k+1) and i_q(k+1) at instant k+1. To avoid switching chatting and to make the controlled variables error approach zero quickly, the proposed sliding-mode function is presented. According to the sliding-mode control theory, the procedure is as follows. The first step is to design the sliding-mode surfaces s_d and s_q.

$$\begin{cases} s_d = i'_d - i_{dm} \\ s_q = i'_q - i_{qm} \end{cases} \tag{15}$$

where i'_d and i'_q denote the estimates of the currents in the dq coordinates, s_d and s_q are sliding-mode surfaces, and i_{dm} and i_{qm} are crude measured currents.

The second step is to design the sliding-mode function. Unlike the traditional sliding-mode function, to make the state-variable error approach zero, the sliding-mode functions v_d and v_q are designed as follows.

$$v_d = k_{kd}\, sat(s_d) + k_{ld} s_d \tag{16}$$

$$v_q = k_{kq}\, sat(s_q) + k_{lq} s_q \tag{17}$$

$$sat(s) = \begin{cases} 1 & \text{if } (s \geq 1) \\ s & \text{if } (s \in (-1, 1)) \\ -1 & \text{if } (s \leq -1) \end{cases} \tag{18}$$

where k_{kd}, k_{kq}, k_{ld}, and k_{lq} denote sliding-mode parameters. The specific selection principle of parameters is introduced in Section III-B.

It should be noted that because the currents measurement error in the d-axis does not lead to torque ripple and motor speed fluctuation, the currents measurement error in the d-axis only leads to flux-weakening control and magnetization control. This paper does not consider the disturbances under the influence of current variation Δi_{dm} between the accurate current i_d and measured current i_{dm}. The current variation Δi_{qm} belongs to the main periodic disturbances that can lead to motor speed fluctuation and pulsating torque T_0, so the predicted disturbances f'_{di} and f'_{qi} under the influence ofcurrent variation Δi_{qm} between the accurate current i_q and measured current i_{qm} are considered in this paper. Therefore, the equations of NCDO can be designed as follows:

$$\begin{cases} U_d = L'_s \dfrac{di'_d}{dt} + R'_s i'_d - \omega_m p L'_s i_{qm} + r'_d - f'_{di} + v_d \\ \dfrac{dr'_d}{dt} = k_{gd} v_d \\ f'_{di} = f'_{di-1} + k_{f3} \dfrac{d\left(\omega_{mi-1} - \omega_{i-1}^{\text{ref}}\right)}{dt} + k_{f4} \dfrac{d\left(\omega_{mi} - \omega_i^{\text{ref}}\right)}{dt} \end{cases} \tag{19}$$

$$\begin{cases} U_q = L'_s \dfrac{di'_q}{dt} + R'_s i'_q + \omega_m p L'_s i_{dm} + \omega_m p \psi'_m + r'_q - f'_{qi} + v_q \\ \dfrac{dr'_q}{dt} = k_{gq} v_q \\ f'_{qi} = f'_{qi-1} + k_{f1} \dfrac{d\left(\omega_{mi-1} - \omega_{i-1}^{\text{ref}}\right)}{dt} + k_{f2} \dfrac{d\left(\omega_{mi} - \omega_i^{\text{ref}}\right)}{dt} \end{cases} \tag{20}$$

where v_d and v_q represent sliding-mode control function; r'_d and r'_q are the estimates of nonperiodic disturbances caused by PMSM parameter mismatch; f'_{di} and f'_{qi} denote the estimates of periodic disturbances caused by ripple current Δi_{qm}; i'_d and i'_q denote the estimates of currents in the dq coordinates; k_{f1}, k_{f2}, k_{f3}, and k_{f4} denote ILC parameters; and k_{gd} and k_{gq} are the SMC disturbance observer parameters.

$$\begin{cases} i'_d(k+1) = \dfrac{T_s}{L'_s} U_d(k) + \left(1 - \dfrac{R'_s T_s}{L'_s}\right) i'_d(k) + T_s \omega_m p i_{qm}(k) \\ \qquad - \dfrac{T_s}{L'_s}(r'_d(k) - f'_{di}(k)) - \dfrac{T_s}{L'_s} v_q(k) \\ r'_d(k+1) = T_s k_{gd} v_d + r'_d(k) \\ f'_{di}(k) = f'_{di-1}(k) + k_{f3} \dfrac{d\left(\omega_m(k)_{i-1} - \omega^{\text{ref}}(k)_{i-1}\right)}{dt} \\ \qquad + k_{f4} \dfrac{d\left(\omega_m(k)_i - \omega^{\text{ref}}(k)_i\right)}{dt} \end{cases} \tag{21}$$

Because the practical system is discrete, the first-order Euler discretization is adopted to acquire the predicted stator currents i_d(k+1) and i_q(k+1), predicted nonperiodic disturbances r'_d(k+1) and r'_q(k+1), and predicted periodic disturbances f'_{di}(k) and f'_{qi}(k). The discrete equation of NCDO can be expressed as Eq.(21).

$$\begin{cases} i'_q(k+1) =_s \dfrac{T_s}{L'_s} U_q(k) + \left(1 - \dfrac{R'_s T_s}{L'_s}\right) i'_q(k) - T_s \omega_m p i_{dm}(k) \\ \qquad - \dfrac{T_s}{L'_s} \psi'_m \omega_m p - \dfrac{T_s}{L'_s}(r'_q(k) - f'_{qi}(k)) - \dfrac{T_s}{L'_s} v_q(k) \\ r'_q(k+1) = T_s k_{gq} v_q + r'_q(k) \\ f'_{qi}(k) = f'_{qi-1}(k) + k_{f1} \dfrac{d\left(\omega_m(k)_{i-1} - \omega^{\text{ref}}(k)_{i-1}\right)}{dt} \\ \qquad + k_{f2} \dfrac{d\left(\omega_m(k)_i - \omega^{\text{ref}}(k)_i\right)}{dt} \end{cases} \tag{22}$$

Because the change in the electrical angle is too slow compared with the system sampling time, the values of f'_{di}(k+1) and f'_{qi}(k+1) are approximately equal to the values of f'_{di}

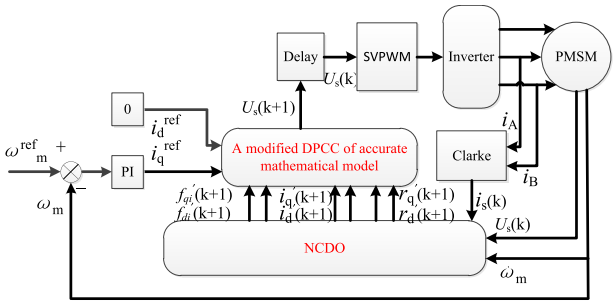

FIGURE 3. The proposed DPCC with NCDO scheme of PMSM drives.

(k) and f'_{qi}(k), respectively. After the NCDO is designed, according to Eq. (12) and Eq. (13), the proposed DPCC with NCDO scheme of PMSM drives is shown in Fig. 3.

Stability Analysis of the Proposed DPCC With NCDO: The stability of analysis of the proposed DPCC with NCDO is introduced in this section. Because NCDO includes the SMC and ILC modules simultaneously, this paper will analyze the two parts. First, this paper analyzes the convergence property in sliding-mode control, and then analyzes the convergence property in the proposed ILC.

To ensure the convergence property of the sliding-mode surface, this paper utilizes the Lyapunov theorem to analyze the observer stability. The Lyapunov function is defined as

$$\mathrm{V} = \frac{1}{2}s^2 \tag{23}$$

To make the function converge, the following equations are used.

$$\begin{cases} \dfrac{d\mathrm{V}_d}{dt} = \dfrac{ds_d}{dt} \cdot s_d \le 0 \\ \dfrac{d\mathrm{V}_q}{dt} = \dfrac{ds_q}{dt} \cdot s_q \le 0 \end{cases} \tag{24}$$

Where $s_d = i'_d - i_{dm}$ and $s_q = i'_q - i_{qm}$. Subtract Eq. (19) and Eq. (20) from Eq. (12) and Eq. (13), and the currents error equation becomes

$$\begin{cases} 0 = L'_s\dfrac{ds_d}{dt} + R'_s s_d + r'_d - r_d - \left(f'_{di} - f_d\right) + \mathrm{v}_d \\ 0 = L'_s\dfrac{ds_q}{dt} + R'_s s_q + r'_q - r_q - \left(f'_{qi} - f_q\right) + \mathrm{v}_q \end{cases} \tag{25}$$

Substituting Eq. (16), Eq. (17), and Eq. (25) into Eq. (24) yields

$$\begin{cases} \dfrac{d\mathrm{V}_d}{dt} = -\dfrac{1}{L'_s}(R'_s s_d + r'_d - r_d - (f'_{di} - f_d) + \mathrm{v}_d)s_d \\ \dfrac{d\mathrm{V}_q}{dt} = -\dfrac{1}{L'_s}(R'_s s_q + r'_q - r_q - (f'_{qi} - f_q) + \mathrm{v}_q)s_q \end{cases}$$
$$= \begin{cases} -\dfrac{1}{L'_s}((R'_s + \mathrm{k}_{ld})s_d^2 + s_d(r'_d - r_d - (f'_{di} - f_d) + \mathrm{k}_{kd}\ sat(s_d))) \\ -\dfrac{1}{L'_s}((R'_s + \mathrm{k}_{lq})s_q^2 + s_q(r'_q - r_q - (f'_{qi} - f_q) + \mathrm{k}_{kq}\ sat(s_q))) \end{cases} \tag{26}$$

According to Eq. (26), in order to make the system stable, k_{kd}, k_{kq}, k_{ld}, and k_{lq} should be satisfied as follows.

$$\mathrm{k}_{ld} > -R'_s \tag{27}$$
$$\mathrm{k}_{lq} > -R'_s \tag{28}$$
$$\mathrm{k}_{kd} > \frac{\left|r'_d - r_d - \left(f'_{di} - f_d\right)\right|}{|s_d|} \tag{29}$$
$$\mathrm{k}_{kq} > \frac{\left|r'_q - r_q - \left(f'_{qi} - f_q\right)\right|}{|s_q|} \tag{30}$$

After the system reaches the sliding-mode surface in a finite time, the errors s_d, s_q and their derivatives can approach zero. B_d and B_q are defined as the variation rates of parameter disturbances r_d and r_q. According to Eq. (19) and Eq. (20), the errors of the disturbances can be simplified as

$$\begin{cases} \dfrac{\mathrm{d}\left(r'_d - r_d\right)}{dt} + B_\mathrm{d} + \mathrm{k}_{gd}\left(r'_d - r_d\right) = 0 \\ \dfrac{\mathrm{d}\left(r'_q - r_q\right)}{dt} + B_\mathrm{q} + \mathrm{k}_{gq}\left(r'_q - r_q\right) = 0 \end{cases} \tag{31}$$

$$\begin{cases} \left(r'_d - r_d\right) = \mathrm{e}^{-\mathrm{k}_{gd}\mathrm{t}}\left[\mathrm{C} + \int B_\mathrm{d}\mathrm{e}^{\mathrm{k}_{gd}\mathrm{t}}\mathrm{dt}\right] \\ \left(r'_\mathrm{q} - r_q\right) = \mathrm{e}^{-\mathrm{k}_{gq}\mathrm{t}}\left[\mathrm{C} + \int B_\mathrm{q}\mathrm{e}^{\mathrm{k}_{gq}\mathrm{t}}\mathrm{dt}\right] \end{cases} \tag{32}$$

where C is a constant. From Eq. (32), it is found that the values of k_{gd} and k_{gq} must be positive.

To ensure the convergence property of ILC, this paper compares the error value of the controlled variable between the ith iteration cycle and the (i+1)th iteration cycle to analyze the observer stability, assuming the motor speed fluctuation is mainly caused by current measurement error and the system has been at steady state for several iteration cycles. To ensure the convergence in ILC, the absolute rotor speed error is defined in Eq. (33). If inequation (34) is satisfied, the system is convergent.

$$\mathrm{e}_{i+1} = \left\|\omega_m(\theta_\mathrm{e})_{i+1} - \omega^{\mathrm{ref}}(\theta_\mathrm{e})_{i+1}\right\| \tag{33}$$
$$\mathrm{e}_{i+1} < \mathrm{e}_i \tag{34}$$

where i+1 represents the (i+1)th iteration cycle, e_{i+1} denotes the absolute value of the rotor speed error at the (i+1)th iteration cycle, and e_i denotes the absolute value of the rotor speed error at the ith iteration cycle. To testify the convergence in ILC, Eq. (4) can become Eq. (35).

$$\int \frac{1}{\eta}\left(1.5p\psi_\mathrm{m}i_q - T_l\right)dt = \omega_m \tag{35}$$

Substitute Eq. (35) into Eq. (33) and Eq. (36) can be presented as

$$\mathrm{e}_{i+1} = \left\|\int \frac{1}{\eta}\left(1.5p\psi_\mathrm{m}i_{qi+1} - T_l\right)dt - \int \frac{1}{\eta}\left(1.5p\psi_\mathrm{m}i^{\mathrm{ref}}_{qi+1} - T_l\right)dt\right\| \tag{36}$$

where $\mathrm{i}_{\mathrm{qi}+1}$ denotes the actual stator current at the (i+1)th iteration cycle, $\mathrm{i}^{ref}_{\mathrm{qi}+1}$ denotes the reference stator current at

the (i+1)th iteration cycle, and Eq. (36) can be turned into Eq. (37) and Eq. (38).

$$e_{i+1} = g_1 \int \left(\left\| i_{qi+1} - i_{qi+1}^{\text{ref}} \right\| \right) dt \tag{37}$$

$$g_1 = \frac{1}{\eta} (1.5 p \psi_m) \tag{38}$$

According to the aforementioned analysis in Eq. (10), the actual current can be presented as Eq. (39).

$$\begin{aligned} i_{qi} &= i_{qmi} - \Delta i_{qmi} \\ &= \left\| i_q^0 \right\|_i + \left\| i_q^1 \right\|_i \sin(\theta_e) + \left\| i_q^2 \right\|_i \sin(2\theta_e) - \Delta i_{qmi} \end{aligned} \tag{39}$$

where i_{qmi} is the measured q-axis current at the ith iteration cycle, $||i_q^0||_i$ denotes the measured q-axis dc-offset currents at the ith iteration cycle, Δi_{qmi} is the ILC current disturbance compensation of the 1st- and 2nd-harmonic current amplitudes of the periodic disturbances at the ith iteration cycle, and i_{qi} is the real q-axis current at the ith iteration cycle after the ILC compensation. Because the current contains a periodic measurement error, $||i_q^1||_i$ and $||i_q^2||_i$ denote the 1st- and 2nd-harmonic current amplitudes of the periodic disturbances at the ith iteration cycle. Because i_{qmi} is a periodic signal, when i_{qi} is steady, the value of i_{qmi} is equal to the value of i_{qmi+1} at the same electrical angle. If the convergence in ILC is satisfied, inequation (40) is as follows.

$$e_{i+1} < e_i = \left\| i_{qi+1} - i_{qi+1}^{\text{ref}} \right\| < \left\| i_{qi} - i_{qi}^{\text{ref}} \right\| \tag{40}$$

Substitute Eq. (39) into inequation (40). Assuming the system only contains the current measurement error, the value of $||i_q^0||_i$ is equal to the value of i_{qi}^{ref}. The inequation can be expressed as follows.

$$\left\| \begin{array}{l} \left\| i_q^1 \right\|_i \sin(\theta_e) + \\ \left\| i_q^2 \right\|_i \sin(2\theta_e) - \Delta i_{qmi} \end{array} \right\| > \left\| \begin{array}{l} \left\| i_q^1 \right\|_{i+1} \sin(\theta_e) + \\ \left\| i_q^2 \right\|_{i+1} \sin(2\theta_e) - \Delta i_{qmi+1} \end{array} \right\| \tag{41}$$

When t=0, the value of Δi_{qmi} is equal to zero. The object of ILC is to generate the value of Δi_{qmi} which is generated by the predicted disturbances f'_{di} and f'_{qi} to counteract the value of $||i_q^1||_i$ and $||i_q^2||_i$ caused by current measurement error. It has been noted that when the value of $||i_q^1||_i$ and $||i_q^2||_i$ is greater than the value of Δi_{qmi} within several iteration cycles, the system does not perform iterative control and the predicted disturbances f'_{di} and f'_{qi} are fixed until the system enters another steady state. Therefore, inequation (42) and inequation (43) can are as follows.

$$\left\| i_q^1 \right\|_i \sin(\theta_e) + \left\| i_q^2 \right\|_i \sin(2\theta_e) > \Delta i_{qmi} \tag{42}$$

$$\left\| i_q^1 \right\|_{i+1} \sin(\theta_e) + \left\| i_q^2 \right\|_{i+1} \sin(2\theta_e) > \Delta i_{qmi+1} \tag{43}$$

In this case, according to Eq. (41)–(43), the condition of convergence can be written as inequation (44) within several iteration cycles.

$$\Delta i_{qmi+1} > \Delta i_{qmi} \tag{44}$$

As for the predicted disturbances $f'_{qi+1}(\theta_e)$, according to Eq. (37), Eq. (20) can be turned into Eq. (45), which is expressed as follows.

$$f'_{qi+1}(\theta_e) = f'_{qi}(\theta_e) + k_{f1} g_1 \left(i_{qi} - i_{qi}^{\text{ref}} \right) + k_{f2} g_1 \left(i_{qi+1} - i_{qi+1}^{\text{ref}} \right) \tag{45}$$

where $f'_{qi}(\theta_e)$ denotes the predicted periodic disturbances at the ith iteration cycle and θ_e denotes the electrical angle of the periodic disturbances. Substituting Eq. (39) and Eq. (13) into Eq. (45), according the aforementioned analysis, Eq. (46) is as follows.

$$\begin{aligned} & f'_{qi+1}(\theta_e) \\ &= f'_{qi}(\theta_e) + k_{f1} g_1 \left(\left\| i_q^1 \right\|_i \sin(\theta_e) + \left\| i_q^2 \right\|_i \sin(2\theta_e) - \Delta i_{qmi} \right) \\ &\quad + k_{f2} g_1 \left(\left\| i_q^1 \right\|_{i+1} \sin(\theta_e) + \left\| i_q^2 \right\|_{i+1} \sin(2\theta_e) - \Delta i_{qmi+1} \right) \\ &= L_s \frac{d \Delta i_{qmi}}{dt} + R_s \Delta i_{qmi} + \omega_m p L_s \Delta i_{dmi} \\ &\quad + k_{f1} g_1 \left(\left\| i_q^1 \right\|_i \sin(\theta_e) + \left\| i_q^2 \right\|_i \sin(2\theta_e) - \Delta i_{qmi} \right) \\ &\quad + k_{f2} g_1 \left(\left\| i_q^1 \right\|_{i+1} \sin(\theta_e) + \left\| i_q^2 \right\|_{i+1} \sin(2\theta_e) - \Delta i_{qmi+1} \right) \end{aligned} \tag{46}$$

Substituting Eq. (13) into Eq. (46), Eq. (47) is as follows.

$$\begin{aligned} & L_s \frac{d \left(\Delta i_{qmi+1} - \Delta i_{qmi} \right)}{dt} + R_s \left(\Delta i_{qmi+1} - \Delta i_{qmi} \right) \\ &\quad + \omega_m p L_s \left(\Delta i_{dmi+1} - \Delta i_{dmi} \right) \\ &= + k_{f1} g_1 \left(\left\| i_q^1 \right\|_i \sin(\theta_e) + \left\| i_q^2 \right\|_i \sin(2\theta_e) - \Delta i_{qmi} \right) \\ &\quad + k_{f2} g_1 \left(\left\| i_q^1 \right\|_{i+1} \sin(\theta_e) + \left\| i_q^2 \right\|_{i+1} \sin(2\theta_e) - \Delta i_{qmi+1} \right) \end{aligned} \tag{47}$$

If we take the values of the ILC parameter k_{f2} to be equal to the value of the ILC parameter $-k_{f1}$, Eq. (47) becomes Eq. (48).

$$\begin{aligned} & L_s \frac{d \left(\Delta i_{qmi+1} - \Delta i_{qmi} \right)}{dt} + R_s \left(\Delta i_{qmi+1} - \Delta i_{qmi} \right) \\ &\quad + \omega_m p L_s \left(\Delta i_{dmi+1} - \Delta i_{dmi} \right) \\ &= - k_{f2} g_1 \left(\Delta i_{qmi+1} - \Delta i_{qmi} \right) \\ &\quad + k_{f1} g_1 \left(\left\| i_q^1 \right\|_i \sin(\theta_e) + \left\| i_q^2 \right\|_i \sin(2\theta_e) \right) \\ &\quad + k_{f2} g_1 \left(\left\| i_q^1 \right\|_{i+1} \sin(\theta_e) + \left\| i_q^2 \right\|_{i+1} \sin(2\theta_e) \right) \end{aligned} \tag{48}$$

It has been noted that, because this paper does not consider the ILC current disturbance compensation Δi_{dmi} at the ith iteration cycle, the value of $\Delta i_{dmi+1} - \Delta i_{dmi}$ can be taken as zero. Furthermore, because the 1st-and 2nd-harmonic current amplitudes are all generated by the same method of measurement, the values of $||i_q^1||_{i+1}$ and $||i_q^2||_{i+1}$ at the (i+1)th iteration cycle are equal to the values of $||i_q^1||_i$ and

$||i_q^2||_i$ at the ith iteration cycle. In this case, Eq. (49) can also be considered constant.

$$\begin{aligned} C2 = {} & k_{f1}g_1\left(\left\|i_q^1\right\|_i \sin(\theta_e) + \left\|i_q^2\right\|_i \sin(2\theta_e)\right) \\ & - \omega_m p L_s\left(\Delta i_{dmi+1} - \Delta i_{dmi}\right) \\ & + k_{f2}g_1\left(\left\|i_q^1\right\|_{i+1} \sin(\theta_e) + \left\|i_q^2\right\|_{i+1} \sin(2\theta_e)\right) \\ = {} & -\omega_m p L_s\left(\Delta i_{dmi+1} - \Delta i_{dmi}\right) = 0 \end{aligned} \tag{49}$$

Therefore, after substituting Eq. (49) into Eq. (48), Eq. (50) is as follows.

$$\frac{d\left(\Delta i_{qmi+1} - \Delta i_{qmi}\right)}{dt} + \frac{\left(R_s + k_{f2}g_1\right)}{L_s}\left(\Delta i_{qmi+1} - \Delta i_{qmi}\right) = 0 \tag{50}$$

Take the term of Δi_{qmi+1}-Δi_{qmi} as an unknown variable, and Eq. (50) can be solved as follows.

$$\left(\Delta i_{qmi+1} - \Delta i_{qmi}\right) = C1\left(e^{\frac{\left(R_s + k_{f2}g_1\right)}{L_s}t}\right) \tag{51}$$

When t>0, if the condition of convergence can be satisfied as in Eq. (44), C1>0. When t$\to +\infty$, because the value of $\Delta i_{qmi+1} - \Delta i_{qmi}$ is not infinite and slows the increase rate of Δi_{qmi+1}, inequation (52) can be satisfied as follows.

$$\frac{\left(R_s + k_{f2}g_1\right)}{L_s} < 0 \tag{52}$$

It can be found that $k_{f2}g_1 < -R_s$. In this case, according to Eq. (38), the ILC parameters k_{f1} and k_{f2} can be satisfied as follows.

$$k_{f2} < -\frac{R_s}{\frac{1}{\eta}(1.5p\psi_m)} \tag{53}$$

$$k_{f1} > -\frac{R_s}{\frac{1}{\eta}(1.5p\psi_m)} \tag{54}$$

As for determining the ILC parameters k_{f3} and k_{f4}, according to Eq. (37), Eq. (19) can be turned into Eq. (55).

$$f'_{di+1}(\theta_e) = f'_{di}(\theta_e) + k_{f3}g_1\left(i_{qi} - i_{qi}^{ref}\right) + k_{f4}g_1\left(i_{qi+1} - i_{qi+1}^{ref}\right) \tag{55}$$

where $f'_{di}(\theta_e)$ denotes the predicted periodic disturbances at the ith iteration cycle. Similarly, substituting Eq. (39) and Eq. (12) into Eq. (55),

$$\begin{aligned} & L_s\frac{d\left(\Delta i_{dmi+1} - \Delta i_{dmi}\right)}{dt} + R_s\left(\Delta i_{dmi+1} - \Delta i_{dmi}\right) \\ & \quad + \omega_m p L_s\left(\Delta i_{qmi+1} - \Delta i_{qmi}\right) \\ & = +k_{f3}g_1\left(\left\|i_q^1\right\|_i \sin(\theta_e) + \left\|i_q^2\right\|_i \sin(2\theta_e) - \Delta i_{qmi}\right) \\ & \quad + k_{f4}g_1\left(\left\|i_q^1\right\|_{i+1} \sin(\theta_e) + \left\|i_q^2\right\|_{i+1} \sin(2\theta_e) - \Delta i_{qmi+1}\right) \end{aligned} \tag{56}$$

Solve Eq. (56) to obtain Eq. (57).

$$\Delta i_{qmi+1} = \Delta i_{qmi}\frac{\left(\omega_m p L_s - k_{f3}g_1\right)}{\left(\omega_m p L_s + k_{f4}g_1\right)} \tag{57}$$

If the condition of convergence can be satisfied as shown in Eq. (57), the ILC parameters k_{f3} and k_{f4} can be satisfied as follows.

$$\frac{\left(\omega_m p L_s - k_{f3}g_1\right)}{\left(\omega_m p L_s + k_{f4}g_1\right)} > 1 \tag{58}$$

IV. SIMULATION STUDY

The PMSM parameters are listed in Table 1. This paper testifies the correctness of the methods under different conditions through MATLAB software. This paper defines the first method as traditional DPCC, and the second method is the proposed DPCC with NCDO. Considering that the control system contains one-step delay, the delay time is set to one control period and the system sampling time is set to 50 μs. This paper adopts the speed-loop control strategy to drive the PMSM, and the maximum output value of speed controller is limited to 10 A. Because the PMSM is a surface-mount motor, this paper adopts the $i_d = 0$ control strategy to drive the PMSM. The switching frequency is set to 20 kHz and the simulation parameters are $k_{kd} = k_{kq} = 10$, $k_{ld} = k_{lq} = 10$, $k_{gd} = k_{gq} = 830$, and $k_{f1} = 15$, $k_{f2} = -15$, $k_{f3} = 20$, and $k_{f4} = -15$ based on the system stability condition.

TABLE 1. PMSM parameters.

PARAMETER	DESCRIPTION	VALUE
P_N	RATED POWER (KW)	2
P	NUMBER OF POLE PAIRS	4
R_S	STATOR RESISTANCE (Ω)	0.365
L_S	STATOR INDUCTANCE (MH)	1.225
Ψ_M	ROTOR MAGNET FLUX (WB)	0.1667
T_N	RATED TORQUE (NM)	10

First, when the system has no parameter mismatch or current measurement error and the target speed is set to 600 r/min, the two methods almost have the same performance. Fig. 4 shows the current i_A, i_d, and i_q of the two methods from speeds of 0 r/min to 600 r/min and the load torque change from 4 Nm to 6 Nm at 0.15 s when $\Psi'_r = 2\Psi_r$. From (c), it can be found that i_q exceeds 10 A with increasing speed, which means that the q-axis current cannot track the reference current well. When $\Psi'_r = 1/2\Psi_r$, it has the same condition. The total harmonic distortion (THD) computations at different conditions are listed in Table 2.

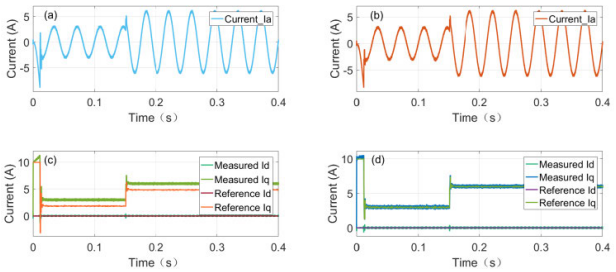

FIGURE 4. Simulation results of i_A phase current, i_d current, and speed under $\Psi'_r = 2\Psi_r$ at 600 r/min: (a), (c) method 1; (b), (d) method 2.

TABLE 2. THD comparisons of two methods in simulation results.

Different conditions	Method 1	Method 2
Without mismatch at 600 r/min	0.68%	0.90%
$L_s^{'} = 2L_s$ at 600 r/min	2.78%	0.91%
$R_s^{'} = 10R_s$ at 600 r/min	8.65%	1.03%
Current offset (1 A) mismatch at 400 r/min	7.98%	4.45%
Current offset (2 A) mismatch at 400 r/min	15.91%	11.41%
$\Psi_r^{'} = 2\Psi_r$ at 600 r/min	7.93%	0.91%
$L_s^{'} = 2L_s$ at 1200 r/min	3.04%	1.00%

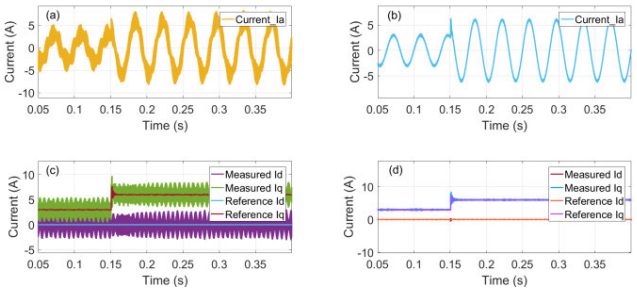

FIGURE 5. Simulation results of i_A phase current, i_d current, and speed under $L_s' = 2L_s$ at 600 r/min: (a), (c) method 1; (b), (d) method 2.

Fig. 5 shows the current comparisons of the two methods under $L_s' = 2L_s$ at 600 r/min from 4 Nm to 6 Nm. From the graph, we can see that the current ripple in method 1 is higher than that in method 2.

To observe the high-speed performance between the two methods, Fig. 6 shows the i_A, i_d, and i_q performance comparisons of the two methods under $L_s' = 2L_s$ at 1200 r/min from 4 Nm to 6 Nm. It can be seen that method 2 has the lowest current ripple.

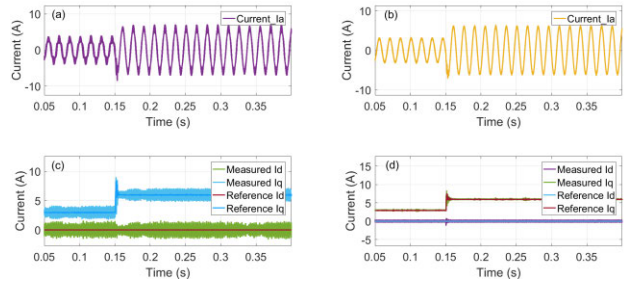

FIGURE 6. Simulation results of i_A phase current, i_d current, and speed under $L_s' = 2L_s$ at 1200 r/min: (a), (c) method 1; (b), (d) method 2.

To verify that the influence of resistance mismatch disturbance in DPCC, Fig. 7 shows the current comparison of the two methods under $R_s' = 10R_s$ at 600 r/min. From this graph, it can be seen that the measured currents can track the reference currents well in method 2, which indicates that method 2 can suppress the resistance mismatch disturbance.

To testify the proposed method possesses the advantage to suppress nonperodic and periodic disturbances, method 2 and

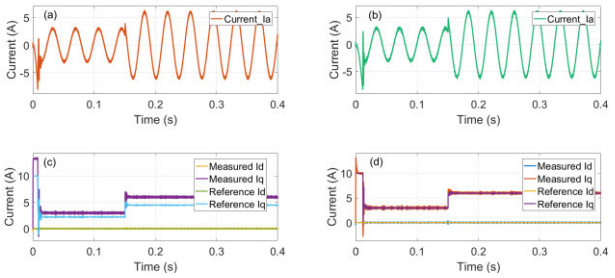

FIGURE 7. Simulation results of i_A phase current, i_d current, and i_q current under $R_s' = 10R_s$ at 600 r/min: (a), (c) method 1; (b), (d) method 2.

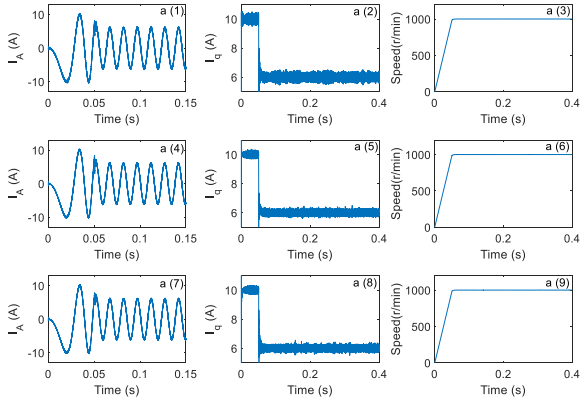

FIGURE 8. Simulation results of i_A phase current, i_d current and speed under $L_s' = 2L_s$ at 1000r/min: (a1), (a2), (a3) method 1; (a4), (a5), (a6) method 2; (a7), (a8), (a9) method 3.

method 3 are redefined as the DPCC with SMC disturbance observer in [18] and proposed method respectively. Fig. 8 shows current i_A, i_q current and speed performance comparisons of three methods under $L_s' = 2L_s$ at 1000r/min. It can be seen that method 3 and method 2 has the same performance, which can testify that method 3 can have the same ability to suppress the nonperiodic disturbance with method 2. In addition to suppressing the PMSM parameter mismatch disturbances, and to testify that method 3 can restrain the current measurement error disturbance, this paper adds a sinusoidal disturbance to the d-axis current i_d and the q-axis current i_q to simulate the periodic harmonic currents. The sinusoidal disturbance's amplitude is set to the value of 1 A and the frequency is same with the PMSM phase's stator currents frequency. It has been noted that because the system is based on speed control, the output in the speed controller can track the measured currents. In this case, the pulsating torque is not obvious. This paper observes the speed error between the target speed and the measured speed performance of the system. Furthermore, the ILC algorithm requires several iteration cycles to estimate the periodic disturbances, so the disturbances are compensated at several iteration cycles. Fig. 9 shows that the PMSM speed error at 400r/min in three methods. From graph (a3) which begins to iterate from 0.05s to 0.4s, ten iterations are carried out, and it can be found that the PMSM speed error decreases with the iteration increasing. Fig. 10 shows that the frequency

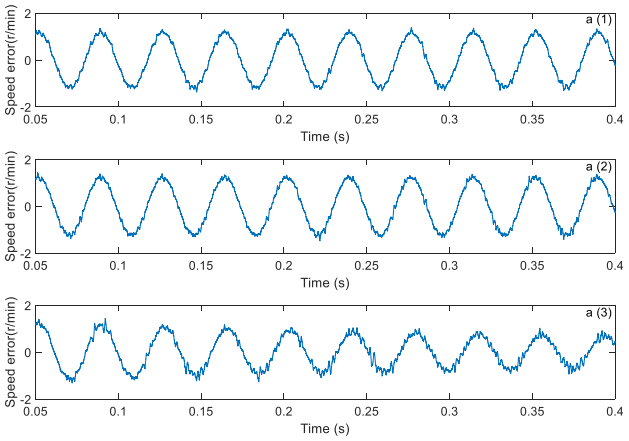

FIGURE 9. Simulation results of motor speed error at 400r/min: (a1) method 1; (a2) method 2; (a3) method 3.

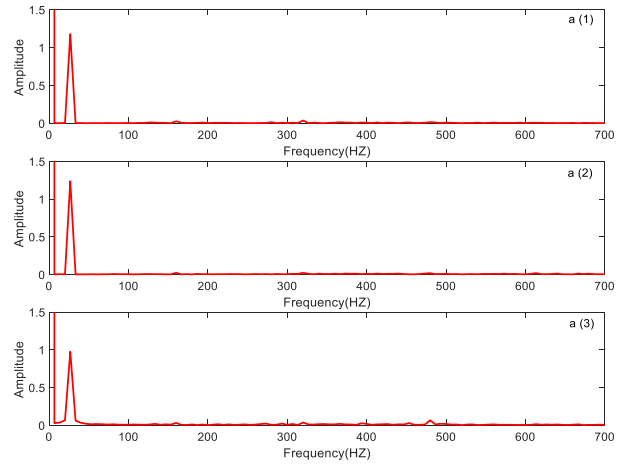

FIGURE 10. Simulation results of the frequency spectrum at 400r/min: (a1) method 1; (a2) method 2; (a3) method 3.

spectrum comparisons of three methods at 400r/min. It can be seen that the amplitude of sinusoidal disturbance frequency is decreased in (a3). In this case, the proposed DPCC can suppress the parameter mismatch disturbances and current measurement error disturbances in simulation, which is better than the method 2 in [18].

V. EXPERIMENTAL RESULTS

In this section, the experimental platform is established. Before describing the performance of the two methods under different conditions, the experimental platform of motor drives is introduced. The platform includes a power supply (400 V), 2-kW drive PMSM, DSP emulator, oscilloscope, Siemens control system that can be taken as a load motor system, drive PMSM controller, and PC. This paper utilizes the TMS320F28377d as the main chip for the PMSM controller and selects the FNC42060F-type IPM as the power devices in the two-level inverter. The PMSM drive system is presented in Fig. 11.

The system sampling period is set to 50 μs, which is the same as in the simulation. The experimental parameters are

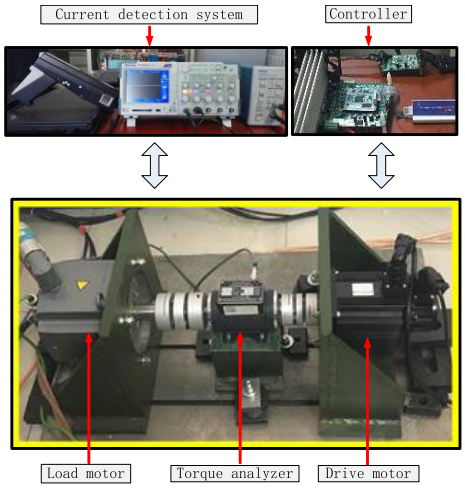

FIGURE 11. Experimental platform of a two-level inverter PMSM drive.

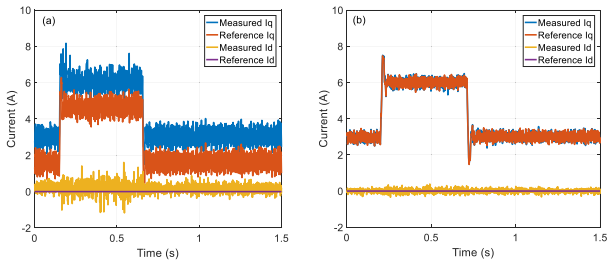

FIGURE 12. Experimental results of i_d current and i_q current under $\Psi_r' = 2\Psi_r$ at 600 r/min: (a) method 1, (b) method 2.

$k_{kd} = k_{kq} = 20$, $k_{ld} = k_{lq} = 20$, $k_{gd} = k_{gq} = 630$, $k_{f1} = 25$, $k_{f2} = -25$, $k_{f3} = 35$, and $k_{f4} = -25$. To observe the transient and steady-state performance of the two methods, the load is set from 3 Nm to 6 Nm and then to 3 Nm during the experiment. When there is no parameter mismatch or current measurement error disturbances, the two methods almost have the same performance in the experimental results. Fig. 12 shows the comparison of the currents of the two methods under $\Psi_r' = 2\Psi_r$ at 600 r/min. From the graph, it can be seen that the current ripple in method 1 (traditional DPCC) is higher than that in method 2 (proposed DPCC), and the measured current i_q can track the reference current i_q in method 2. Similarly, the THD computations at different conditions are listed in Table 3. Fig. 13 shows that current performance of the two methods under $L_s' = 2L_s$ at 600 r/min.

TABLE 3. THD comparisons of two methods in experimental results.

Different conditions	Method 1	Method 2
Without mismatch at 600 r/min	7.33%	7.50%
$L_s' = 2L_s$ at 600 r/min	49.53%	6.19%
$R_s' = 10R_s$ at 600 r/min	14.65%	8.28%
Current offset (1 A) mismatch at 400 r/min	15.33%	8.40%
Current offset (2 A) mismatch at 400 r/min	26.28%	11.67%
$\Psi_m' = 2\Psi_m$ at 600 r/min	17.41%	10.67%
$L_s' = 2L_s$ at 1200 r/min	34.43%	11.04%

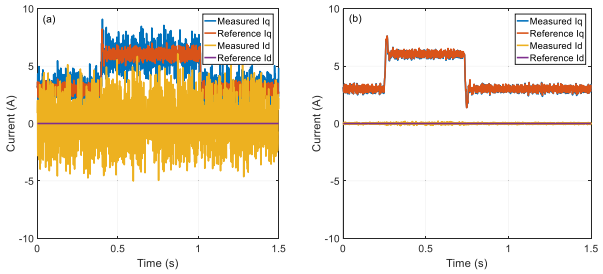

FIGURE 13. Experimental results of i_d current and i_q current under $L'_s = 2L_s$ at 600 r/min: (a) method 1, (b) method 2.

It can be seen that the current ripple in method 1 is smaller than that in method 2.

To demonstrate the high-speed condition, Fig. 14 shows the i_d and i_q performance comparisons of the two methods under $L'_s = 2L_s$ at 1200 r/min. It can be seen that the currents ripple is lower in method 2, which indicates that the method can suppress inductance mismatch disturbances.

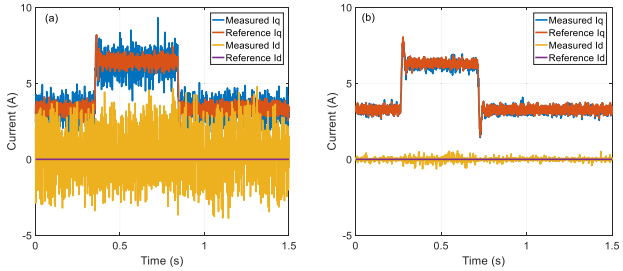

FIGURE 14. Experimental results of i_d current and i_q current under $L'_s = 2L_s$ at 1200 r/min: (a) method 1, (b) method 2.

For $R'_s = 10R_s$ at 600 r/min, Fig. 15 shows the currents of the two methods. It can be seen that the measured current i_q cannot track the reference current i_q in method 1, and the currents ripple is too high compared with the current performance in method 2.

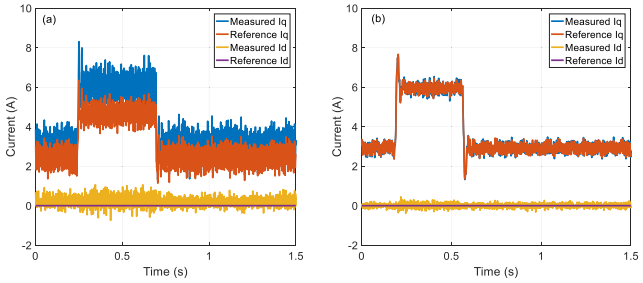

FIGURE 15. Experimental results of i_d current and i_q current under $R'_s = 10R_s$ at 1200 r/min: (a) method 1, (b) method 2.

To observe the i_A performance in the two methods under $L'_s = 2L_s$ at 600 r/min, the load torque is set from 2 Nm to 5 Nm. From Fig. 16, which was graphed by oscilloscope, it can be seen that the i_A ripple in method 1 is too high.

Furthermore, the multiple-parameter mismatch test is carried out in this paper. When the PMSM parameters are under

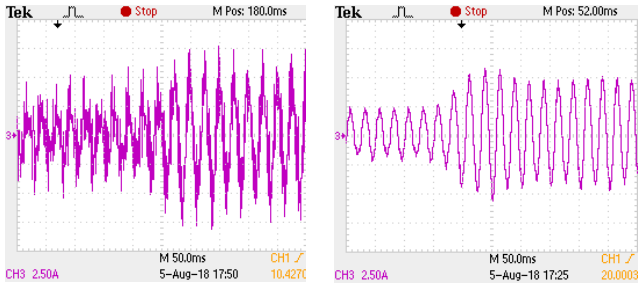

FIGURE 16. Experimental results of i_A current under $L'_s = 2L_s$ at 600 r/min: the left is method 1; the right is method 2.

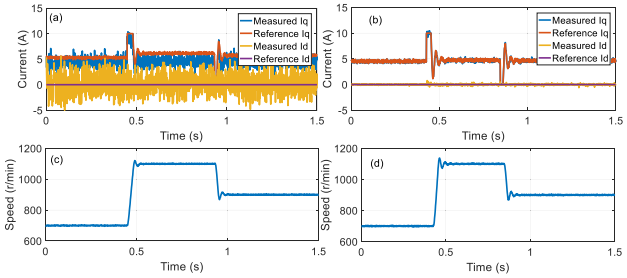

FIGURE 17. Experimental results of i_d current, i_q current, and motor speed under $R'_s = 5R_s$, $L'_s = 2L_s$, and $\Psi'_r = 0.5\Psi_r$: (a), (c) method 1; (b), (d) method 2.

the $R'_s = 5R_s$, $L'_s = 2L_s$, and $\Psi'_r = 0.5\Psi_r$ condition, the current and PMSM speed performance of the two methods are shown in Fig. 17. The torque ripple is set to 5 Nm at all times. The speed target is set from 700 r/min to 1100 r/min, and then decreased from 1100 r/min to 900 r/min. From this result, we can see that method 2 can suppress the parameters mismatch disturbances.

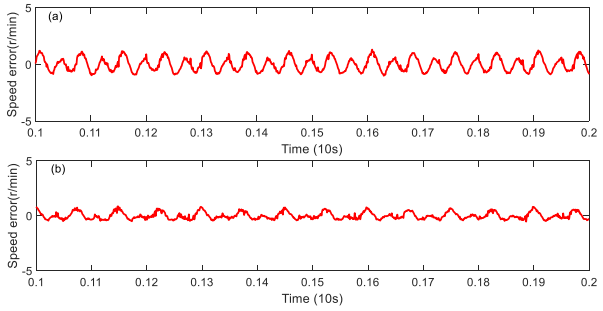

FIGURE 18. Experimental results of the motor speed error under 1-A current-offset disturbance: (a) method 1; (b) method 2.

To establish the current measurement error disturbance in DPCC, the dc-offset current disturbance (current values of 1 A and 2 A) are added into the system. The frequency of the periodic offset currents is the same as the motor phase's stator current frequency. Fig. 18 and Fig. 19 show the PMSM speed error performance under 1-A and 2-A dc-current offset disturbances at 400 r/min for the two methods. Because the sampling data is limited, after ten iteration cycles are over,

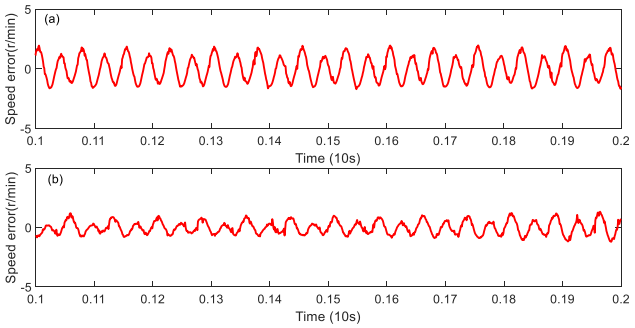

FIGURE 19. Experimental results of the motor speed error under 2-A current-offset disturbance: (a) method 1; (b) method 2.

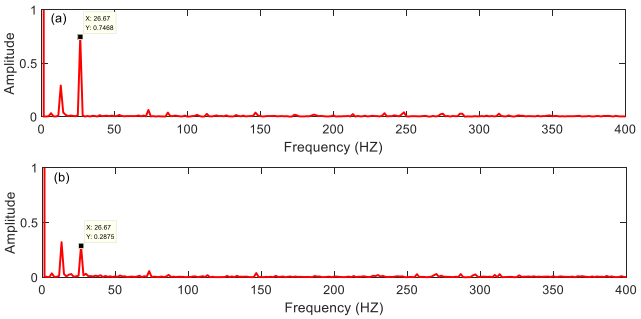

FIGURE 20. Experimental results of the frequency spectrum under 1-A current-offset disturbance: (a) method 1; (b) method 2.

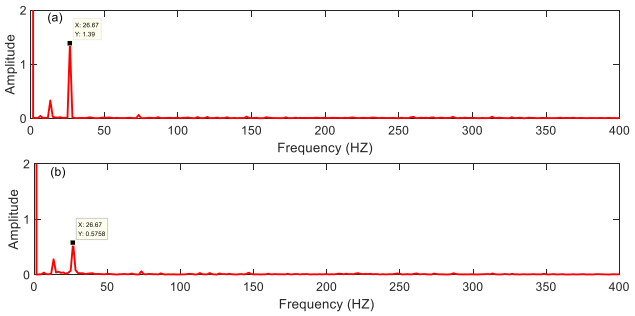

FIGURE 21. Experimental results of the frequency spectrum under 2-A current-offset disturbance: (a) method 1; (b) method 2.

the data is measured through the PC. In this case, we can see that the speed error is small in method 2. Fig. 20 and Fig. 21 depict the frequency spectrum of the two methods under 1-A and 2-A current offset. It can be seen that the amplitude of the 26.67-Hz signal, which is at the same frequency as the PMSM phase's stator current at 400 r/min, is reduced from 0.7468 to 0.2875 under a 1-A current-offset disturbance. Similarly, the amplitude of the 26.67-Hz signal is reduced from 1.39 to 0.5758 under a 2-A current-offset disturbance. Therefore, from the experimental result, the proposed DPCC with NCDO not only suppresses the influence of parameter mismatch disturbances but also suppresses the influence of current measurement error disturbances.

VI. CONCLUSION

From the simulation and experimental results, under conditions without parameter mismatch disturbance, it can be found that the traditional DPCC and the proposed DPCC with NCDO have the same performance. When parameter mismatch disturbances occur, the proposed DPCC with NCDO is able to suppress the influence of the disturbance and reduce the current harmonic. Apart from that, when there are periodic disturbances such as current measurement error disturbances in the system, the proposed DPCC with NCDO can also compensate. Therefore the proposed DPCC with NCDO can be experimentally applied to PMSM drives.

REFERENCES

[1] M. Alizadeh and S. S. Kojori, "Augmenting effectiveness of control loop of a PMSG based wind energy conversion system by a virtually adaptive PI controller," *Energy*, vol. 91, pp. 610–629, Nov. 2015.

[2] B.-J. Kang and C.-M. Liaw, "A robust hysteresis current-controlled PWM inverter for linear PMSM driven magnetic suspended positioning system," *IEEE Trans. Ind. Electron.*, vol. 48, no. 5, pp. 956–967, Oct. 2001.

[3] R. Errouissi, M. Ouhrouche, W.-H. Chen, and A. M. Trzynadlowski, "Robust cascaded nonlinear predictive control of a permanent magnet synchronous motor with antiwindup compensator," *IEEE Trans. Ind. Electron.*, vol. 59, no. 8, pp. 3078–3088, Aug. 2012.

[4] J. Hou, J. Sun, and H. Hofmann, "Adaptive model predictive control with propulsion load estimation and prediction for all-electric ship energy management," *Energy*, vol. 150, pp. 877–889, May 2018.

[5] A. P. M. Reza and M. H. Ali, "An optimized SVPWM switching strategy for three-level NPC VSI and a novel switching strategy for three-level two-quadrant chopper to stabilize the voltage of capacitors," *Energy*, vol. 35, no. 12, pp. 4917–4931, Dec. 2010.

[6] J. Beerten, J. Verveckken, and J. Driesen, "Predictive direct torque control for flux and torque ripple reduction," *IEEE Trans. Ind. Electron.*, vol. 57, no. 1, pp. 404–412, Jan. 2010.

[7] C.-K. Lin, T.-H. Liu, J.-T. Yu, L.-C. Fu, and C.-F. Hsiao, "Model-free predictive current control for interior permanent-magnet synchronous motor drives based on current difference detection technique," *IEEE Trans. Ind. Electron.*, vol. 61, no. 2, pp. 667–681, Feb. 2014.

[8] C.-K. Lin, J.-T. Yu, Y.-S. Lai, and H.-C. Yu, "Improved model-free predictive current control for synchronous reluctance motor drives," *IEEE Trans. Ind. Electron.*, vol. 63, no. 6, pp. 3942–3953, Jun. 2016.

[9] J. Talla, V. Q. Leu, V. Smidl, and Z. Peroutka, "Adaptive speed control of induction motor drive with inaccurate model," *IEEE Trans. Ind. Electron.*, vol. 65, no. 11, pp. 8532–8542, Mar. 2018.

[10] M. H. Holakooie, M. Ojaghi, and A. Taheri, "Direct torque control of six-phase induction motor with a novel MRAS-based stator resistance estimator," *IEEE Trans. Ind. Electron.*, vol. 65, no. 10, pp. 7685–7696, Oct. 2018.

[11] K.-H. Kim and M.-J. Youn, "A nonlinear speed control for a PM synchronous motor using a simple disturbance estimation technique," *IEEE Trans. Ind. Electron.*, vol. 49, no. 3, pp. 524–535, Jun. 2002.

[12] M. Siami, D. A. Khaburi, A. Abbaszadeh, and J. Rodríguez, "Robustness improvement of predictive current control using prediction error correction for permanent-magnet synchronous machines," *IEEE Trans. Ind. Electron.*, vol. 63, no. 6, pp. 3458–3466, Jun. 2016.

[13] M. Siami, D. A. Khaburi, and J. Rodíguez, "Torque ripple reduction of predictive torque control for PMSM drives with parameter mismatch," *IEEE Trans. Power Electron.*, vol. 32, no. 9, pp. 7160–7168, Sep. 2017.

[14] L. He, F. Wang, J. Wang, and J. Rodriguez, "Zynq implemented lunenberger disturbance observer based predictive control scheme for PMSM drives," *IEEE Trans. Power Electron.*, to be published. doi: 10.1109/TPEL.2019.2920439.

[15] J. Wang, F. Wang, G. Wang, S. Li, and L. Yu, "Generalized proportional integral observer based robust finite control set predictive current control for induction motor systems with time-varying disturbances," *IEEE Trans. Ind. Informat.*, vol. 14, no. 9, pp. 4159–4168, Sep. 2018.

[16] X. Zhang, L. Sun, K. Zhao, and L. Sun, "Nonlinear speed control for PMSM system using sliding-mode control and disturbance compensation techniques," *IEEE Trans. Power Electron.*, vol. 28, no. 3, pp. 1358–1365, Mar. 2013.
[17] Y. Jiang, W. Xu, C. Mu, and Y. Liu, "Improved deadbeat predictive current control combined sliding mode strategy for PMSM drive system," *IEEE Trans. Veh. Technol.*, vol. 67, no. 1, pp. 251–263, Jan. 2018.
[18] X. Zhang, B. Hou, and Y. Mei, "Deadbeat predictive current control of permanent-magnet synchronous motors with stator current and disturbance observer," *IEEE Trans. Power Electron.*, vol. 32, no. 5, pp. 3818–3834, May 2017.
[19] T. M. Jahns and W. L. Soong, "Pulsating torque minimization techniques for permanent magnet AC motor drives-a review," *IEEE Trans. Ind. Electron.*, vol. 43, no. 2, pp. 321–330, Apr. 1996.
[20] B. Le Pioufle, "Comparison of speed nonlinear control strategies for the synchronous servomotor," *Electr. Mach. Power Syst.*, vol. 21, no. 2, pp. 151–169, Sep. 1993.
[21] L. Li, Y. Liu, Z. Yang, X. Yang, and K. Li, "Mean-square error constrained approach to robust stochastic iterative learning control," *IET Control Theory Appl.*, vol. 12, no. 1, pp. 38–44, Jan. 2018.
[22] D. C. Hanselman, "Minimum torque ripple, maximum efficiency excitation of brushless permanent magnet motors," *IEEE Trans. Ind. Electron.*, vol. 41, no. 3, pp. 292–300, Jun. 1994.
[23] J.-X. Xu, S. K. Panda, Y.-J. Pan, T. H. Lee, and B. H. Lam, "A modular control scheme for PMSM speed control with pulsating torque minimization," *IEEE Trans. Ind. Electron.*, vol. 51, no. 3, pp. 526–536, Jun. 2004.
[24] I.-C. Baik, K.-H. Kim, and M.-J. Youn, "Robust nonlinear speed control of PM synchronous motor using boundary layer integral sliding mode control technique," *IEEE Trans. Control Syst. Technol.*, vol. 8, no. 1, pp. 47–54, Jan. 2000.
[25] J. Liu, H. Li, and Y. Deng, "Torque ripple minimization of PMSM based on robust ILC via adaptive sliding mode control," *IEEE Trans. Power Electron.*, vol. 33, no. 4, pp. 3655–3671, Apr. 2018.
[26] P. Cortes, J. Rodriguez, C. Silva, and A. Flores, "Delay compensation in model predictive current control of a three-phase inverter," *IEEE Trans. Ind. Electron.*, vol. 59, no. 2, pp. 1323–1325, Feb. 2012.

XIN YUAN was born in Heilongjiang, China, in 1990. He received the B.Eng. and M.Sc. degrees in electrical engineering, in 2013 and 2016, respectively. He is currently pursuing the Ph.D. degree with the National Engineering Laboratory for Electric Vehicles and School of Mechanical Engineering, Beijing Institute of Technology.

His research interests include synchronous motor drives and multi-phase motor drives.

SHUO ZHANG received the B.Eng. degree from the North China Institute of Aerospace Engineering, Hebei, China, in 2011, and the Ph.D. degree in vehicle engineering from the Beijing Institute of Technology, Beijing, China, in 2017.

He is currently an Assistant Professor with the National Engineering Laboratory for Electric Vehicles and School of Mechanical Engineering, Beijing Institute of Technology. His research interests include the modeling and control for the permanent magnet synchronous motor, multi-motor driving system, and hybrid power system.

CHENGNING ZHANG received the M.E. degree in control theory and control engineering and the Ph.D. degree in vehicle engineering from the Beijing Institute of Technology, Beijing, China, in 1989 and 2001, respectively.

He is currently a Professor and the Vice Director of the National Engineering Laboratory for Electric Vehicles, Beijing Institute of Technology. His research interests include electric vehicles, vehicular electric motor drive systems, battery management systems, and chargers.